Chapter 3. Plasma Simulations and Diagnostics

3.1 Plasma Simulation

3.1.1 The Particle-in-cell Method

The particle-in-cell (PIC) plasma simulation method uses computers to simulate the motion of charged particles in a plasma (Birdsall and Longdon, 1991). Even a low density plasma can have millions of particles per cubic centimeter, so PIC simulations do not attempt to solve for the motion of all the particles in a given plasma problem, but rather only a subset of so called "super particles". PIC simulation codes generally start with the Lorentz force equation on a particle (Birdsall and Longdon, 1991),

$$\frac{d\vec{P}_k}{dt} = \frac{q_k}{m_k}\left(\vec{E} + \vec{v}_k \times \vec{B}\right) \tag{3.1}$$

where $\vec{P}_k$ is the particle momentum, q_k/m_k is the charge to mass ratio, $\vec{E}$ is the electric field, $\vec{v}_k$ is the velocity, $\vec{B}$ is the magnetic field, and k indicating particle species. The momentum is then related to the velocity by

$$\vec{P}_k = \frac{m_k \vec{v}_k}{\sqrt{1 - \vec{v}_k \cdot \vec{v}_k / c^2}} \tag{3.2}$$

For non relativistic particles,

$$\vec{P}_k \approx m_k \vec{v}_k = m_k \frac{d\vec{r}_k}{dt} \tag{3.3}$$

where $\vec{r}_k$ is the particle position. Each particle has a charge Q_k associated with it. In order to solve (3.1), the E and B fields are needed and are obtained by solving Maxwell's equations. In a linear, isotropic medium Maxwell's equations and the continuity equation are

$$\nabla \times \vec{E} = -\frac{\partial \vec{B}}{\partial t}, \tag{3.4}$$

$$\nabla \times \vec{H} = \frac{\partial \vec{D}}{\partial t} + \vec{J} \tag{3.5}$$

$$\nabla \cdot \vec{D} = \rho \tag{3.6}$$

$$\nabla \cdot \vec{B} = 0 \tag{3.7}$$

$$\nabla \cdot \vec{J} = -\frac{\partial \rho}{\partial t} \tag{3.8}$$

where

$$\vec{D} = \varepsilon \vec{E} \tag{3.9}$$

$$\vec{B} = \mu \vec{H} \tag{3.10}$$

and J, ε, μ and ρ are known functions of space and time. In (3.5), J is the sum of particle currents and conduction currents ($J_c = \sigma E$). Thus, this set of equations comprises a self-consistent model for the temporal and spatial evolution of both the fields and particles.

3.1.2 The XOOPIC Code

The X-Windows version of the Object-Oriented Particle-in-Cell known as XOOPIC code was chosen for the discharge simulation. XOOPIC version 2.51 is a two-dimensional relativistic electromagnetic particle-in-cell code written in C++ by J.P. Verboncoeur and collaborators at the University of California at Berkeley (Verboncoeur et al, 1995). The code uses cartesian and cylindrical geometries and can handle electrostatic and electromagnetic simulations and relativistic and non-relativistic particles. It was designed to be user-friendly with a sophisticated graphical user interface (GUI) and an expert system advisor. The particles follow the relativistic equation of motion in electric and magnetic fields and then constitute a source current for the field equations. The particles are advanced using the relativistic time-center Boris scheme (Birdsall and Longdon, 1991). The code uses a charge conservation current weighting algorithm.

3.1.3 The Simulation Set Up

The simulation model for our rf driven multicusp ion source is presented schematically in figure 3.1 The model is an axisymmetric cylinder 10 cm in diam and 9 cm long with 32x64 grid sizes along the r and z space. The plasma boundary is assumed to be ideal conducting walls. The code runs on a Linux server using X11 as X-Windows server. The parameters including Grid, Control, Species, Conductor or Dielectric and Port with generic boundary parameters were set as an input file (see Appendix B2). The multicusp magnetic field produced by permanent magnets of the ion source was generated by using MS Fortran PowerStation 4.0 to create a table of the field values. The field of each mesh point is then read from the file as specified in the Control group. The field value is similar to that calculated by the MAGNUS code which assumed zero field in ϕ and z axes. The Monte Carlo calculation on particle-particle interaction and particles with background gas was also included. Since it was considered as an inductive discharge, the rf field at 13.56 MHz was launched as a PortTM. An ElectrostaticFlag = 0 was added in the Control group to enforce the simulation using the electromagnetic field solver only.The simulations were then carried out with Ar gas at pressure of 10 mTorr (MCC group) and an applied rf amplitude of 25 V which is equal to an rf power of 500 W at 1.25 ohms antenna impedance (Port group). The secondary electron emission factor from the plasma electrode boundary was set to 0.2 and reduced to 0.1 for the ion source wall boundary. These emission values have to be set to include exact electron fluxes to the plasma generation processes. The time step was as low as 3×10^{-12} s (Control group) and was found to depend very strongly on grid sizes under the Courant limit constraint $c\Delta t < (1/\Delta z^2+1/\Delta r^2)^{-1/2}$. Note: The computer running time was more than 3 days for few hundreds ns simulating time.

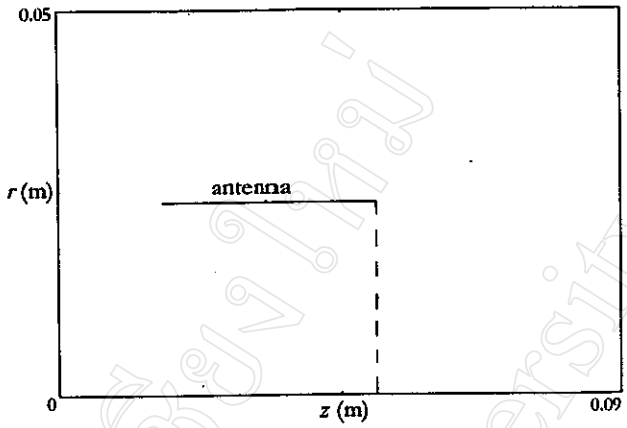

Fig. 3.1 Schematic diagram of the simulation model with cylindrical shaped boundary 10 cm diam and 9 cm long. The z-axis is taken as the symmetry axis.

3.1.4 The Simulation Results

The results of XOOPIC simulation are shown in Fig.3.2. In Fig. 3.2(a) the calculated particles density is plotted with time. Fig. 3.2(b) shows the magnetic field inside the volume due to the input magnetic cusp field distributed in r-z space. Fig. 3.2(c) shows the profile of electron density in r-z space where Fig. 3.2(d) shows that of Argon. All profiles were acquired after 373 ns which is about five times the radio frequency period. These profiles seem to be stable after this elapsed time, in which the system could be considered as approaching the steady state. Starting with an initial particle density of 10^{16} m^{-3}, density in the field-free zone grew at least two orders of magnitude to 10^{18} m^{-3}. Due to the limited time range considered, the actual steady state has not yet been reached and it can be seen that the number of particles represented in Fig. 3.2(a) continuing to increase exponentially. The magnetic field inside the source chamber in Fig. 3.2(b) has the effect of an added localized field due to

the rf-induction over the field-free region. In this simulation, it is shown that the localized field in the "field free" zone is very small, less than 0.015 Tesla. The particle density in r-z space as shown in Fig. 3.2(c) and (d) is distributed uniformly along the entire radial axis except near the edge where a strong magnetic field exists. Electrons are clearly seen to be confined in the field free zone. In a simulation without a magnetic field the particle density was found to be non-uniform along the radial axis with very low plasma density. Moreover, the average kinetic energy of electrons is much lower in the case of magnetic confinement.

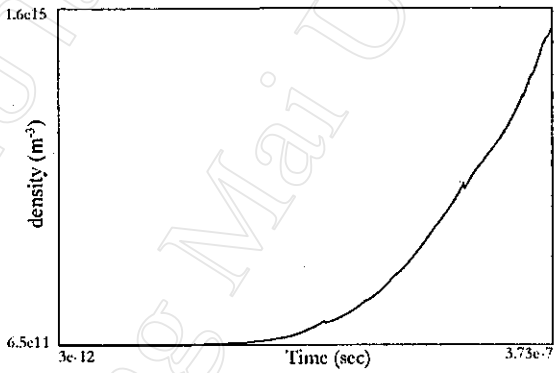

a)

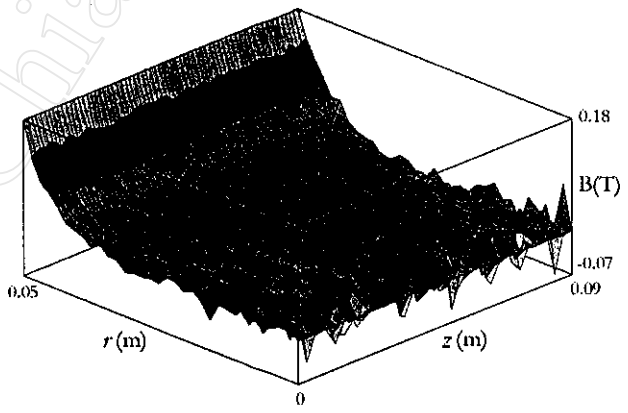

b)

Fig. 3.2 XOOPIC simulation results in r-z space at 10 mTorr base pressure: (a) the calculated particles density against time; (b) the magnetic field inside the source volume

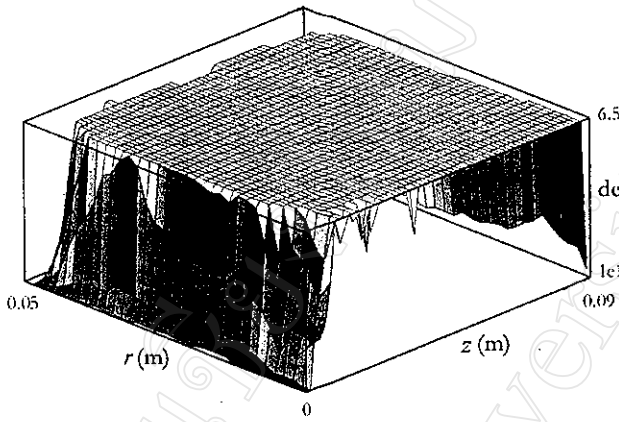

c)

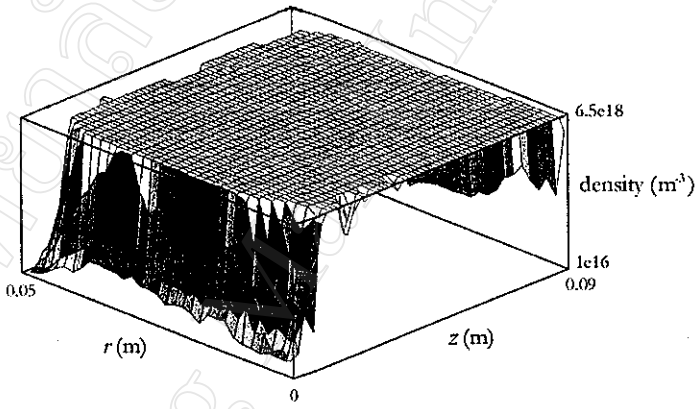

d)

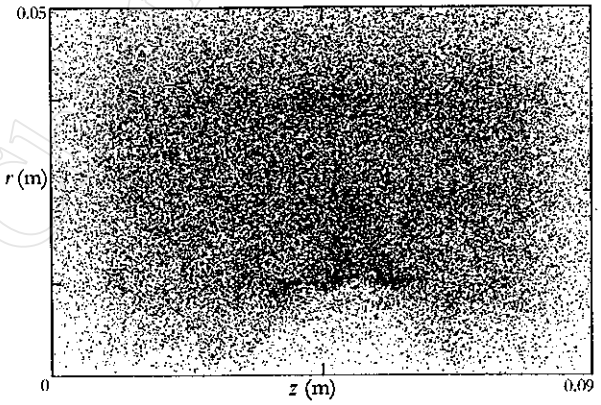

e)

Fig. 3.2 XOOPIC simulation results in r-z space at 10 mTorr base pressure: (c) profile of the electron density (d) profile of the ion density; (e) electron distribution

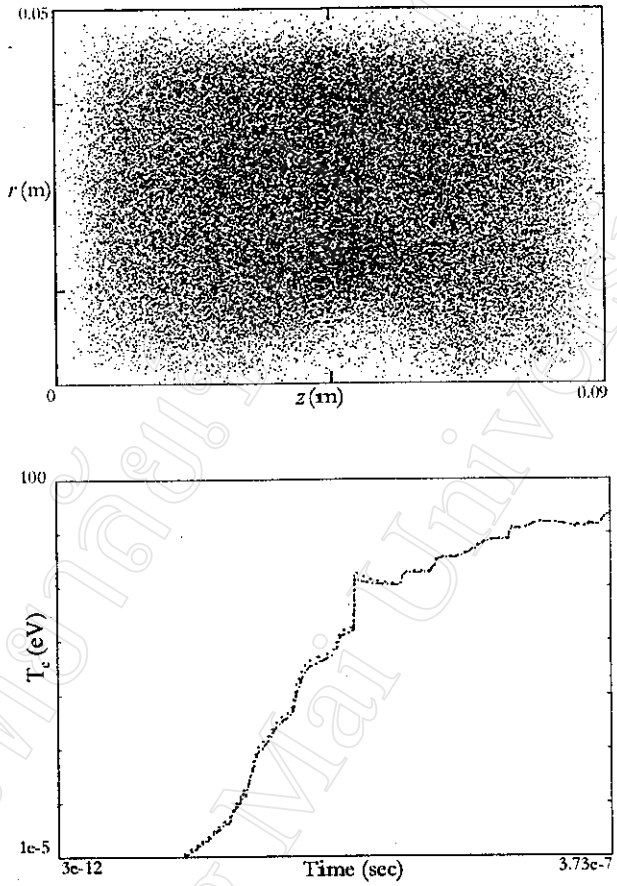

Fig. 3.2 XOOPIC simulation results in r-z space at 10 mTorr base pressure: (f) ion distribution; (g) T_e profiles against time. All data are taken at 373 ns revolution time

Fig. 3.2(e) and (f) give a clearer picture of the particle distribution for electron and Argon in r-z space, respectively. It can be distinctly seen that the electron density near the magnetic wall has been significantly affected by the strong magnetic field much more than that of Argon in which the particle is heavier. The distorted distribution near the antenna may be due to a high fluctuation of an induced rf field direction along the z-axis which can be seen

from the E-field plot (not shown here). This causes a distorted Poynting vector because the plasma-rf power absorption near this region is probably not uniform. Even though, the number of particles in 3.2(a) did not yet reach a steady state, the graph of electron temperature T_e against time in Fig. 3.2(g) approaches a stable value with an average T_e of about 10 eV.

3.2 Optical Emission Spectroscopy

Optical emission spectroscopy (OES) is a valuable tool for the study of plasma generating and processing. Gas-phase species are promoted to excited electronic states by collisions with energetic electrons. It is important to note that only excited species in plasma can be detected by OES, and thus the observed spectrum only gives information about the density of atoms in an excited state and no information about the ground state atoms. The densities of excited state species are typically less than 10^{-4} of the ground state density (Lichtenberg, 1985). Still, when such emission is present from the source, OES has proven to be a very powerful and efficient diagnostic tool for the investigation of plasma characteristics. Other technique such as the Langmuir probe can give information only about an integrated ion current for all ion species and charge states.

3.2.1. Quantitative Description of Optical Emission

Based on the assumption that the excited state is formed solely by electron impact excitation and that this excitation occurs in a single step from ground state and emission occurs once the state is excited, optical emission intensity could be written as (Lichtenberg, 1985)

$$I(I_{ij}) = NP_{ij} A_{ij} (I_{ij})K \qquad (3.11)$$

where i indicates the ground state, j indicates the excited state, l_{ij} is the transition wave-length between state i and state j, N is the ground state density, A_{ij} is the Einstein emission probability, K is a correction factor which describes the effect of view volume and alignment, and P is the electron impact excitation function which represents the probability of exciting the state j from the ground state by electron impact. P is a complex function of electron temperature T_e, and is given by (Lichtenberg, 1985)

$$P = \int_0^\infty 4\pi u^2 du \sigma_\lambda(u) u \, f_e(u, T_e, n_e) \tag{3.12}$$

where u is the electron velocity, σ_λ is the cross section for emission of a photon of wave-length λ due to electron impact excitement, and f_e is the electron distribution function which depends on electron temperature and electron density. It is also important to note that the electron temperature is a monotonically increasing function of $1/P_r$, where P_r is the pressure. Among these variables in (3.12), only the ground state density N and the electron impact excitation function P are dependent on the machine settings, and only N is wavelength-independent. The electron temperature is then estimated using a relative intensity method of the spectral lines. The intensity ratio of two lines belonging to the same atomic species and same ionization level is given by (Azam et al, 1998)

$$I_1/I_2 = [A_1 g_1 \lambda_2 / A_2 g_2 \lambda_1] \exp[-(E_1 - E_2)/kT_{ex}] \tag{3.13}$$

where E is transition energy, k is Boltzman constant and T_{ex} is an excited electron temperature. The inverse slope of $ln\ (I/gA)$ plotted against E renders the electron temperature.

3.2.2. OES Experimental Setup

Optical emission spectroscopy involves the collection, spectral dispersion, and detection of light. Typical experimental setups for OES measurements are shown in Fig. 3.3. Emission from a specific volume in the plasma chamber is imaged onto the entrance slit of a spectrometer by a series of UV-grade fused-silica lens and optical fiber. The spectrometer used is the Ocean Optics S2000 Fiber Optic Spectrometer. The internal optics are a miniaturized version of a cross-Czerny-Turner optical bench with 25 μm entry slit. The diffraction grating of 600 lines per mm blazed to maximize first-order diffraction (m=1) at 400 nm. The spectral resolution due to dispersion is given by (Ocean Optics, 2000)

$$\Delta\lambda = (w \cos\theta_m)/m\upsilon f \qquad (3.14)$$

where w is the exit slit width, υ is grating grooves per millimeter and f is the spectrometer focal length which is the distance from the exit slit to the last focusing mirror (also the distance from the entrance slit to the first focusing mirror). The optical resolution of 0.3 nm full width at half maximum (FWHM). The dispersed light is detected by a charged-coupled device (CCD) array detector. This technique can detect a wide spectral range without scanning the grating, thereby giving information rapidly about any changes in plasma luminosity with time. Readout of all 2048 CCD pixels can be done within 3 msec (minimum integration time). Spectral resolution can be improved by examining a smaller spectral range with the same detector, or using a high-density CCD array. The spectrometer interfaces to a PC through an ADC1000 eight-channel, 12-bit, 1 Msample/s ADC card. The emission spectrum is integrated for 50-500 msec to gain its density. The emission lines from 200 to 800 nm were collected,

corrected and analysed by a computer program OOIBase32 which is supplied by Ocean Optics.

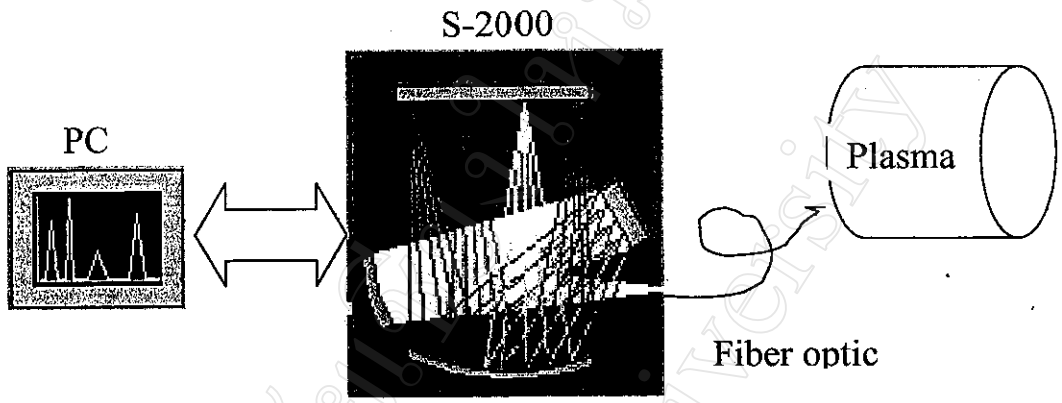

Fig. 3.3 OES measurement setup using Ocean Optics S2000 spectrometer

3.3 Rf-compensated Langmuir Probe

Conceptually, a Langmuir probe consists of a conductor immersed in plasma. By changing the voltage on the probe and measuring the collected current, a complete I-V trace can be acquired, from which important plasma parameters can be derived. Principal among these are the plasma potential, floating potential, plasma density, and electron temperature. (Chen, 1984) In some cases the entire electron energy distribution can be obtained. By characterizing the plasma as a function of pressure, gas composition, sputtering target material, magnetron power, rf power, and position, an understanding can be gained of what effects these variables have on the plasma.

In rf plasma, the probe measurement is affected by the rapidly varying voltages from the induced rf current which leads to variation in plasma potential. For an uncompensated Langmuir probe in an rf plasma, the plasma to probe voltage or so called sheath potential varies in time. The probe then samples an

increasingly large portion of the electron energy distribution. If the plasma potential is varying, the current-voltage relationship obtained is a convolution of the proper curve with the variation in plasma potential. These problems can be avoided by compensating the probe tip (Hiden, 1996). When the probe voltage is far below the plasma potential, the current collected on the probe changes slowly with increasing voltage and there is no difference between the compensated or uncompensated I-V curve. However, at probe voltages closer to the plasma potential, the variation in the sheath voltage leads to large difference in the slope of the log of the electron current plot and can result in an overestimate of electron temperature.

3.3.1 Fabrication of an Rf-Compensated Langmuir Probe

The Langmuir probe is made by threading a coaxial cable through vacuum compatible metal tubing. At the end of the tubing, the cable is cut and a piece of tungsten wire is spot welded as a probe tip to the center conductor. The end of the tubing is sealed, leaving the probe tip exposed to the plasma. The outer conductor of the cable serves as shielding to reduce noise and is critical in an RF plasma. A probe tip diameter of 150 microns and a length of 1 cm is useful. As an rf-compensated probe, a compensated electrode is placed near the probe tip in order to present a variation rf voltage with the same phase as the collecting voltage. Rf compensation is introduced into probes to force the probe tip to follow the fluctuations in the plasma. A perfectly compensated probe would then measure the current as a function of the difference between the tip and background plasma potentials without any time averaging of the rf fluctuations. Since the probe is used in an environment in which metal is being deposited on all surfaces, measures must be taken to prevent the probe tip from shorting to the RF compensation electrode behind it. The probe tip's connection

to the rest of the probe is protected by a hollow ceramic sheath as shown in the schematic close up of the probe tip region in Fig. 3.4 and the photo of an actual Langmuir probe is in Fig. 3.5.

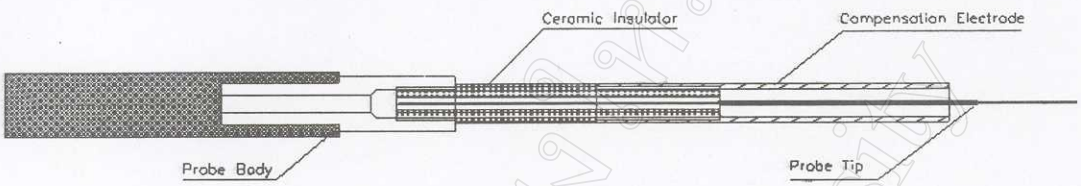

Fig. 3.4 Rf-compensated Langmuir probe schematic

Fig. 3.5 Photo of a self-built rf-compensated Langmuir probe. The probe tip is set to 90 degree for radial profile measurement within ± 4.5 cm range

3.4 OES and Langmuir Probe Setup and Results

The ion source is characterized in terms of radial profile of plasma density n(r). The mean free path for electron-neutral collisions in this experiment is 4-10 cm or longer which is of the order of the source geometry. Long confined

electron trajectories caused by the line cusp boundaries increase the electron residence time and ionization rate. In the case of rf discharge, ionization is caused by energetic electron, and so the electron temperature of the plasma is an important factor. In general, the electron temperature depends on gas pressure as well as input rf power. One has to know the electron temperature since in low-energy ion beam of the 1 keV class, the ion temperature is a main factor for beam divergence while for beams of tens of keV, the non uniformity of the plasma density is the main factor (Ishikawa, 1998).

For OES measurement, the setup is as shown schematically in Fig. 3.6. Optical spectra in the range from 200 to 800 nm were recorded via a 2-meter length fiber optic cable with UV collimating lens through quartz window view-ports by an Ocean Optics S2000 Fiber Optic Spectrometer (model I2J1353). An additional quartz lens with 30 mm focal length was placed close to the windows. The spectrometer was interfaced to a PC through an ADC1000 eight-channel 12-bit 1 Msamples/s card. The sensitivity of the spectrometer was somewhat wavelength dependent and has been corrected with the help of an HgAr calibration light source (Rhodes et al, 2000). The spectral resolution was about 0.3 nm. An integration time of 50 - 500 msec was used to record the emission spectra. For density profile, measurements have been made using a movable rf-compensated Langmuir probe in the same setup. A tungsten cylindrical probe of 150 μm diam with 10 mm length encapsuled in an aluminum sleeve for rf-compensation was used. The probe tip is immersed in the plasma close to the plasma electrode side and perpendicularly moved for radial profile determination. The data have been analysed by software supplied by Hiden Analytical (Hiden, 1996). The plasma density profile was measured along the radial direction for a 9 cm source diameter.

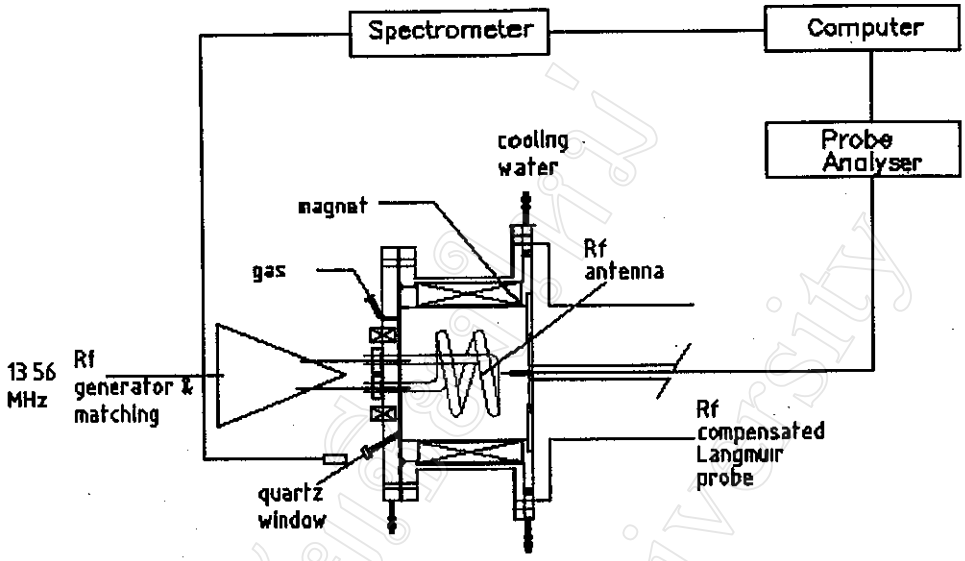

Fig. 3.6 OES and Langmuir probe measurements setup

3.4.1 OES Results

The OES results to determine plasma properties such as ion species, line intensity and electron temperature of each species are shown in Fig. 3.7 a) for 400-550 nm of the composition of excited neutral and ionized Argon lines, b) line intensity as a function of rf power and c) line intensity as a function of argon gas pressure.

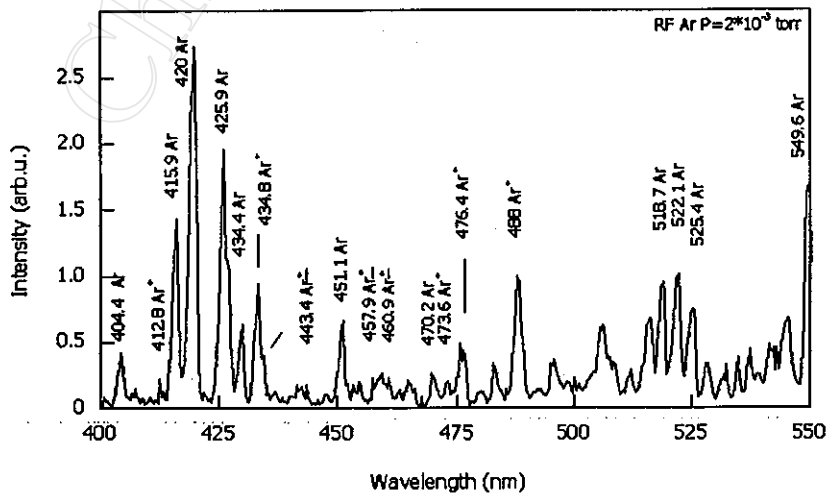

Fig. 3.7 a) OES spectrum of argon plasma at 2 mTorr 200 watts rf power

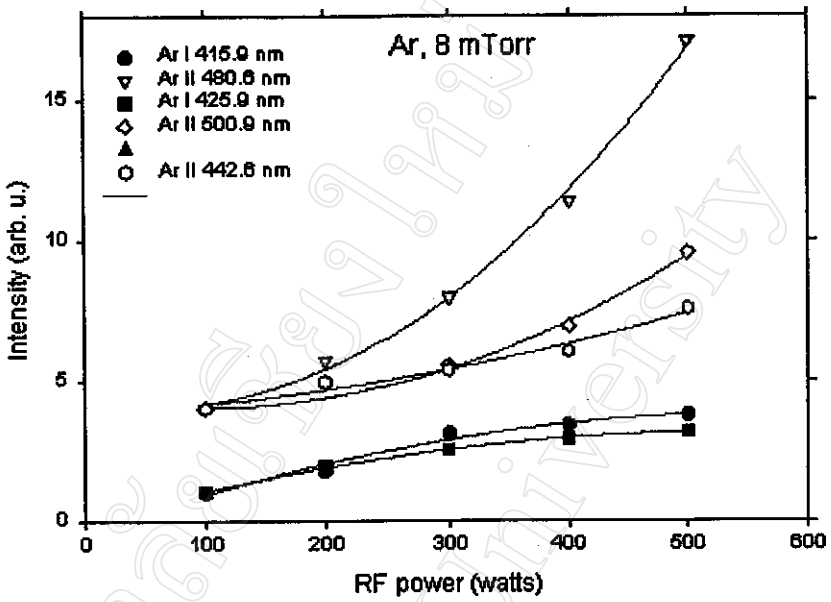

Fig. 3.7 b) line intensity as a function of rf power at 8 mTorr Argon pressure

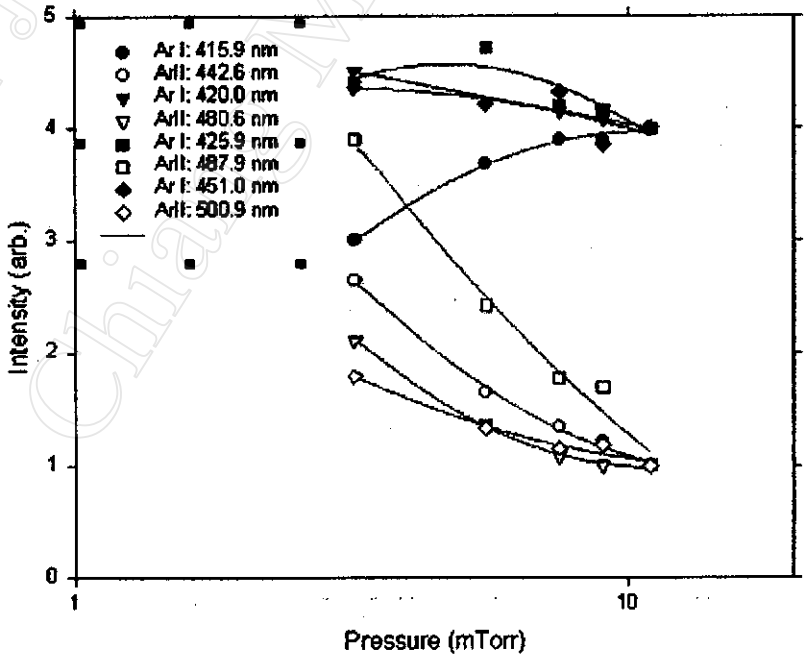

Fig. 3.7 c) line intensity as a function of argon gas pressure at 400 watts rf power

In Fig. 3.7 b) the intensity of some lines corresponding to neutral and ionized species are plotted as a function of rf power. It can be seen that neutral Ar peak becomes saturated while those of Ar ions increase with increasing rf power. This is the known mechanism as rf discharge is mainly due to electron impact excitation-ionization process. Fig. 3.7 c) shows that the intensities of the lines belonging to excited neutral atomic species are higher than for ion species, especially at high pressure. This dependency can be explained as the reduction of mean electron temperature with increasing pressure which will be discussed in the following section.

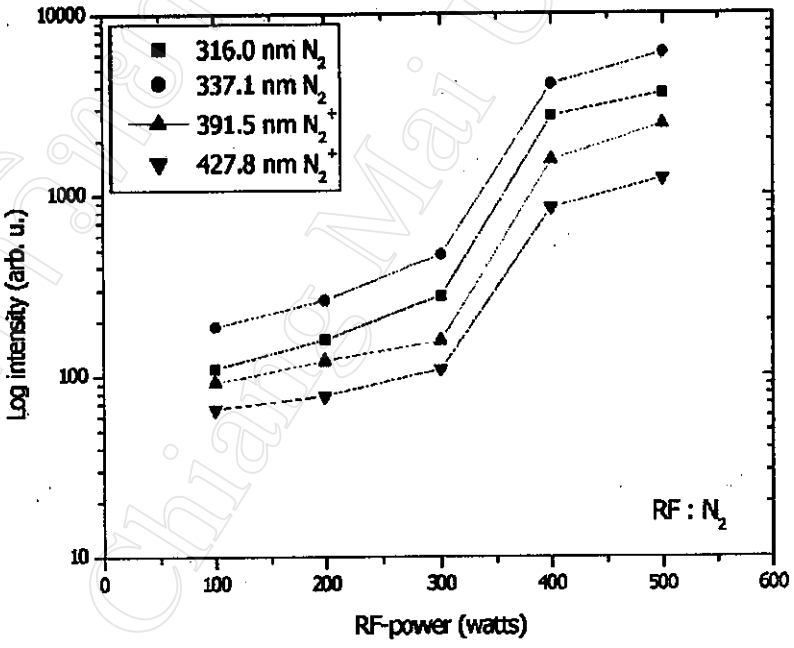

Fig. 3.8 Mode jump in N_2 discharges as the discharge mechanism changes from capacitive to inductive: at 8 mTorr

In Fig. 3.8 as in the range of 300 – 400 watts the intensities of the lines rapidly increase showing an "intensity jump". This jump corresponds to the known phenomena of mode change from the capacitive to the inductive

discharge when the power exceeds a threshold level. The density of electrons rapidly increases 50-100 times more in the inductive discharge mode, as observed by the Langmuir probe measurement (Suzuki et al, 1998), which is in good agreement with our measurement. Thus, the intensity jump was found to be almost 100 times for all atomic and molecular spectral lines. Moreover, one can assume that the excited electron temperature, T_{ex}, of rf-discharge is slightly dependent on rf power. This assumption is justified because, for neutral and ion species the slope of each lines follows similar pattern when the discharge mode changes.

3.4.2 Langmuir Probe Results

Fig. 3.9 shows a typical I-V curve from 8 mTorr Argon plasma at P_{rf} = 200 W. Electron temperature T_e is determined from the slope of the rising curve where ion density is obtained from an ion saturation current and a probe area. Fig. 3.10 shows the density profile along the radial direction of the source. It is fairly uniform (± 8 %) within the plasma diameter of 6 cm then decreases rapidly at the source wall. Such a distribution could be attributed to the magnetic cusp fields which confine electrons in the plasma region. Compared with the measurement of Menard et al (1996) our uniformity variation is about 2 % higher due to a well known behavior that plasma uniformity variation reduces at low operating pressure. Also, this experiment indicates less uniformity of Argon gas than diatomic gas like H_2 or N_2 as observed by others (Menard et al, 1996) under the same gas pressure. For N_2 pressure at 8 mtorr with P_{rf} = 200 W, density deviates about 2 %. Differences in uniformity can be attributed to the availability of multiple long-lived excited energy states of neutral diatomic gas.

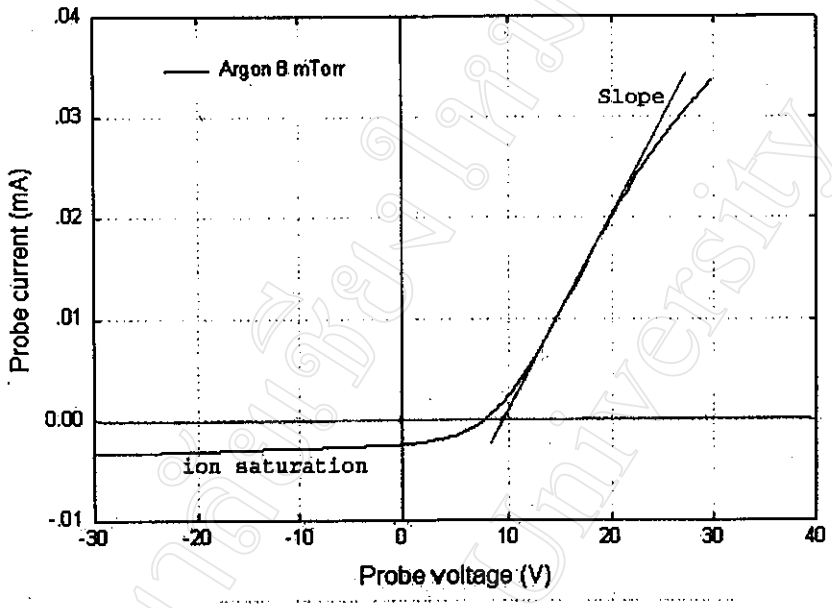

Fig. 3.9 A typical probe I-V curve from Argon plasma at P_{rf} = 200 W

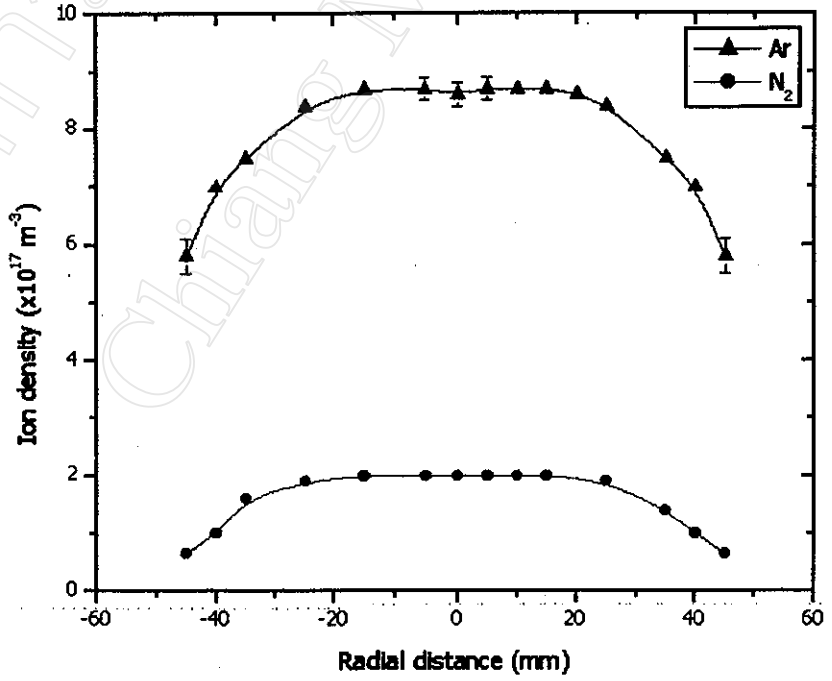

Fig. 3.10 Density profile in the radial direction 1 cm from the antenna

The plasma density of up to 1.5 x 10^{18} m^{-3} can be obtained at 500 W rf power. In comparison with the simulated results, one can see that the plasma density reaches and remains at a value of 10^{18} m^{-3} almost instantly after a few rf cycles. Fig. 3.11 illustrates the variations of the electron temperature T_e against the base pressure at 200 W. The electron temperature (1-3 eV) is found to be relatively independent of the source radius and slightly increases with rf power. The higher electron temperature at a rf power below 200 W is due to a transition from capacitive coupling to inductive coupling. These results also agree with other experiments (Gudmundsson et al, 1997; Yang et al, 1999) for linear decreasing of T_e as a function of log P for cylindrical inductive discharge. T_e was not measured at lower pressure due to an unignitable condition as mentioned in the previous work (Boonyawan et al, 1999). It can also be noted that T_e value is much lower than that predicted by the XOOPIC calculation. In addition, the need to use a filter magnet for separating the plasma excitation and extraction region in this range of rf excitation power may not be necessary because of the low value of T_e.

Also, Fig. 3.11 shows a comparison plot of electron temperature measured by the OES (T_{ex}) and the Langmuir probe (T_{in}). The following lines, belonging to neutral excited Ar atoms, have been chosen: 394.9, 404.4, 415.9, 420.07, 425.9, 427.2, 451.07, 549.6, 555.9, 560.7and 641.6 nm. The data on the transition probabilities: *A*, statistical weights: *g* and energies: *E* of upper levels were taken from (Lide, 1994; NIST, 2001) as shown some in Table 3.1. It is seen that even in the relatively narrow pressure range from 2 to 10x10^{-3} torr, T_{in} and T_{ex} decrease by about 25 % with increasing gas pressure. Also, the value of T_{ex} is about 20 % lower than T_{in} which agree with the literature data (Lieberman and Lichtenberg, 1994). It can also be noted that at different pressures T_{in} was

almost constant in the range between 50 and 500 watts of rf power resulting from present of the multicusp field.

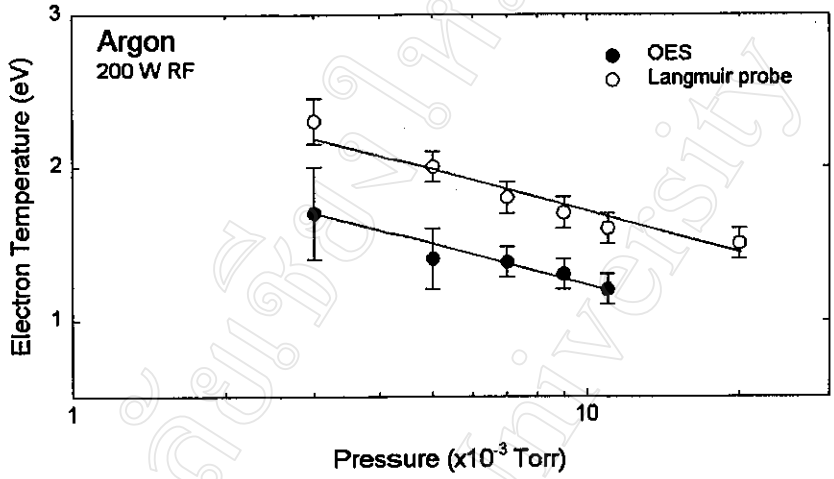

Fig. 3.11 Decreasing of electron temperature with log of pressure measured by Langmuir probe (top) and OES (bottom)

Table 3.1 Data of transition probabilities: *A*, statistical weights: *g* and energies: *E* of upper levels

λ (nm)	$A \times 10^5 (s^{-1})$	*g*	*E* (eV)
394.8	4.55	3	14.215
404.4	3.33	5	14.216
415.9	14.0	5	14.06
420.07	9.67	7	14.033
549.6	16.9	9	14.84
555.9	14.2	5	14.65
560.7	22.2	3	14.63
641.6	11.6	5	14.36